

Article

Optimization of Blue Photorefractive Properties and Exponential Gain of Photorefraction in Sc-Doped Ru:Fe:LiNbO₃ Crystals

Lei Xu and Guanying Chen * 

MIT Key Laboratory of Critical Materials Technology for New Energy Conversion and Storage, School of Chemistry and Chemical Engineering & State Key Laboratory of Urban Water Resource and Environment & Key Laboratory of Micro-Systems and Micro-Structures, Ministry of Education, Harbin Institute of Technology, Harbin 150001, China; xulei82@163.com

* Correspondence: chenguanying@hit.edu.cn

Abstract: Sc:Ru:Fe:LiNbO₃ crystals were grown from congruent melt by using the Czochralski method. A series of LiNbO₃ crystals (Li/Nb = 48.6/51.4) with 0.1 wt% RuO₂, 0.06 wt% Fe₂O₃ and various concentrations of Sc₂O₃ were prepared. RF1 and RF4 refers to the samples containing 0 mol% Sc₂O₃ and 3 mol% Sc₂O₃, respectively. The photorefractive properties of RF4 were measured by Kr⁺ laser ($\lambda = 476$ nm blue light): $\eta_s = 75.7\%$, $\tau_w = 11$ s, $M/\# = 19.52$, $S = 2.85$ cmJ⁻¹, $\Gamma = 31.8$ cm⁻¹ and $\Delta n_{max} = 6.66 \times 10^{-5}$. The photorefractive properties of five systems (η_s , $M/\#$, S , Γ and Δn_{max}) under 476 nm wavelength from RF1 to RF4 continually increased the response time, while τ_w was continually shortened. Comparing the photorefractive properties of Sc (1 mol%):Ru (0.1 wt%):Fe (0.06 wt%):LiNbO₃ measured by Kr⁺ laser ($\lambda = 476$ nm blue light) with Sc (1 mol%):Fe (0.06 wt%):LiNbO₃ measured by He-Ne laser (633 nm red light), η_s increased by a factor of 1.9, V_w (response rate) increased by a factor of 13.9, $M/\#$ increased by a factor of 1.8 and S increased by a factor of 32. The Δn_{max} improved by a factor of 1.4. A strong blue photorefraction was created by the two-center effect and the remarkable characteristic of being in phase between the two gratings recorded in shallow and deep trap centers. The photorefractive properties (η_s , τ_w , $M/\#$, S , Δn_{max}) were increased with an increase in Sc³⁺ ion concentration. Damage-resistant dopants such as Sc³⁺ ions were no longer resistant to damage, but they enhanced the photorefractive properties at the 476 nm wavelength. The experimental results clearly show that Sc-doped two-center Ru:Fe:LiNbO₃ crystal is a promising candidate blue photorefractive material for volume holographic storage. Sc-doped LiNbO₃ crystal can significantly enhance the blue photorefractive properties according to the experimental parameters. Therefore, the Sc:Ru:Fe:LiNbO₃ crystal has better photorefractive properties than the Ru:Fe:LiNbO₃ crystal.



Citation: Xu, L.; Chen, G.

Optimization of Blue Photorefractive Properties and Exponential Gain of Photorefraction in Sc-Doped Ru:Fe:LiNbO₃ Crystals. *Crystals* **2022**, *12*, 1059. <https://doi.org/10.3390/cryst12081059>

Academic Editor: Maria Milanova

Received: 27 June 2022

Accepted: 19 July 2022

Published: 29 July 2022

Publisher's Note: MDPI stays neutral with regard to jurisdictional claims in published maps and institutional affiliations.



Copyright: © 2022 by the authors. Licensee MDPI, Basel, Switzerland. This article is an open access article distributed under the terms and conditions of the Creative Commons Attribution (CC BY) license (<https://creativecommons.org/licenses/by/4.0/>).

Keywords: Sc:Ru:Fe:LiNbO₃ crystal; photorefractive properties; volume holographic storage

1. Introduction

Fe-doped lithium niobate single crystals, LiNbO₃:Fe, have been grown intentionally since the 1960s as a material for the holographic recording of information [1–6]. Fe-doped LiNbO₃ crystals are one of the most widely used photorefractive materials in volume holographic storage due to their high diffraction efficiency, high data storage density and long storage lifetime. This is because the impurities of Fe can improve the photorefractive effect of LiNbO₃ crystals. However, several shortcomings, such as a long response time, low sensitivity and strong light-induced scattering, hinder the applications of Fe:LiNbO₃ crystals in optical holographic storage [2–5]. Recent studies demonstrated that a Ru ion can play a similar role [7,8]. Simultaneous doping of Fe and Ru tends to produce a better photorefractive effect of the LiNbO₃. Indeed, two kinds of such ions were incorporated into LiNbO₃ crystals to yield Ru:Fe:LiNbO₃ crystals in order to realize nonvolatile holographic storage.

It was also demonstrated that doping other types of impurity ions can improve the resistance ability of LiNbO₃ crystals for optical damage [9–15]. A set of optical damage resistance dopants, including In, Mg, Zn, Sc and Hf, were doped into the crystal for such a purpose [16]. Among them, Sc³⁺ ion impurity is the most effective due to the lower threshold concentration, which was reported to be about 3.0 mol%. As a result, Sc³⁺ doping has been widely investigated to produce high-quality Sc-doped LiNbO₃ crystals with a large diameter and high optical quality. Recent studies found that the optical damage resistivity of doped ions also depends on the incident light wavelength. Qiao et al. [17] found that the UV (351 nm) photorefraction of a LiNbO₃ crystal doped with In, Zn or Na was enhanced significantly compared to the nominally pure LiNbO₃ crystal. To date, almost all enhanced photorefraction is investigated using UV light in single-center-doped LiNbO₃ crystals.

Considering the improved photorefractive ability of LiNbO₃ crystals by doping Ru and Fe, as well as the improved optical damage resistance by doping Sc, it will be of great interest to investigate the photorefractive properties of two-center-doped LiNbO₃ crystals, i.e., Sc:Ru:Fe:LiNbO₃, to reveal the role of Sc doping. Moreover, in addition to the use of UV light, using other wavelengths for photorefractive investigation will also be interesting.

Thus, based on the considerations above, two-center Sc:Ru:Fe:LiNbO₃ crystals were grown using the Czochralski method. The incident light wavelength was selected as 476 nm (blue light), which has enough energy to excite the charge carriers' holes of the Sc:Ru:Fe:LiNbO₃ crystals [18]. It was established experimentally that the blue photorefraction of the Ru:Fe:LiNbO₃ doped with Sc was enhanced significantly compared to Sc:Ru:Fe:LiNbO₃ crystals. Sc³⁺ ions play a special role in blue photorefraction. Sc:Ru:Fe:LiNbO₃ crystals exhibit excellent properties such as a high refractive index change, high sensitivity, large exponential gain coefficient Γ and dynamic range, together with a fast response time at the 476 nm wavelength.

2. Experiments

Crystal Growth and Sample Preparation

Using the Czochralski method, a series of LiNbO₃ crystals were grown from congruent melts (Li/Nb = 48.6/51.4) in the air atmosphere along the *c* direction. The raw materials used for crystal growth were Li₂CO₃, Nb₂O₅, Sc₂O₃, RuO₂ and Fe₂O₃. RuO₂ and Fe₂O₃ content in the melt was 0.1 and 0.03 wt%, respectively. Sc₂O₃ content in the melt was 0, 0.5, 1.0 and 1.5 mol%. The raw materials were mixed for 12 h. Mixtures were heated at 750 °C for 2 h to remove CO₂ and then further heated up to 1150 °C for 2 h to form polycrystalline powder. The optimum growth conditions were as follows: an axial temperature gradient of 40–50 K/cm, rotating rate of 10–25 rpm and pulling rate of 0.5–2 mm/h. The grown crystals were polarized at 1200 °C with a current density of 5 mA/cm². The crystal was cut into Y-cut plates (10 × 2 × 10 mm) (X × Y × Z) with polished surfaces at a doping concentration as shown in Table 1.

Table 1. The doping concentration of Ru:Fe:LiNbO₃ crystal.

Sample	RF1	RF2	RF3	RF4
[Sc ₂ O ₃] in melt (mol%)	0	0.5	1.0	1.5
[RuO ₂] in melt (wt%)	0.1	0.1	0.1	0.1
[Fe ₂ O ₃] in melt (wt%)	0.03	0.03	0.03	0.03

3. Results and Discussion

3.1. Type of Dominant Charge Carriers

Figure 1a,b show the erasing processes in sample RF3, with both signal light (S) and reference light (R), for two different lasers with wavelengths of 476 nm and 633 nm, respectively, which were utilized to determine the dominant carrier type. The diffraction efficiency is normalized for comparison. As shown in Figure 1a, when erasing with the 476 nm light, the decay time of the R erasing is much slower than that of the S erasing, implying that the light energy transfer is unidirectional from R to S. This energy transfer

direction is the same as the direction of the optical axis of the crystal, indicating holes are the dominant charge carriers. In comparison, when erasing with 633 nm light as shown in Figure 1b, the decay time of R is much faster than that of S, implying the electrons are the dominant charge carriers. The dominant charge carriers depend on the laser wavelength. At 476 nm, Ru is a shallow trap, and Fe is a deep trap center. The blue light of 476 nm has enough energy to excite holes from both the shallow and deep trap centers, so holes become the dominant charge carriers. At 633 nm, Fe is the shallow trap center, and Ru is the deep trap center. Because the red light of 633 nm can only excite electrons from the shallow trap but not from the deep trap centers, they become the dominant charge carrier [19].

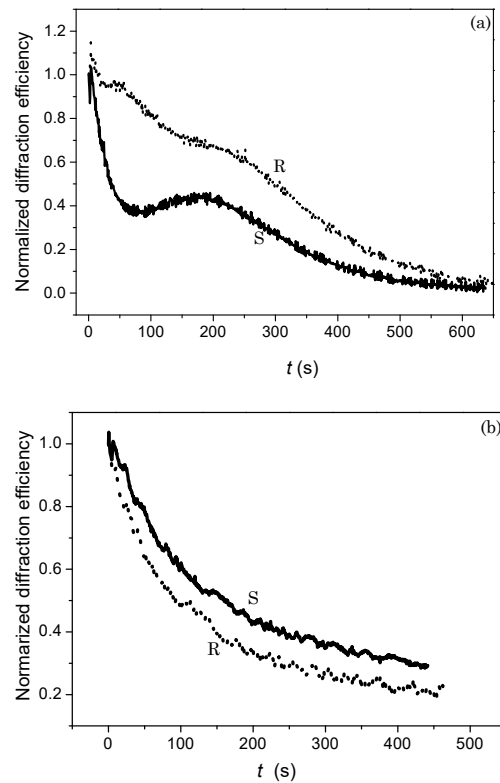


Figure 1. Erase curves of as-grown state Sc:Ru:Fe:LiNbO₃ crystal at (a) 476 nm wavelength and (b) 633 nm wavelength.

3.2. Measurement of Exponential Gain Coefficient in Sc:Ru:Fe:LiNbO₃ Crystal

The exponential gain coefficient of a photorefractive crystal reflects the ability of the energy to transition from the pump light to the signal light during the information storage process. The larger the coefficient is, the greater the multiplicity of the signal light that is amplified. Thus, the signal light becomes clearer during its reappearance, and greater diffraction efficiency can be obtained. Therefore, the exponential gain coefficient is one of the important guidelines for evaluating the photorefractive effect.

3.3. Calculation Formulas of the Exponential Gain Coefficient

The intensity of the signal beam and pump beam with coupling can be achieved by solving the coupling-wave equation. The result is expressed below:

$$I_1(\delta) = \frac{I_1(0) + I_2(0)}{I_1(0) + I_2(0) \exp(\Gamma\delta)} \exp(\Gamma - a)\delta \quad (1)$$

$$I_2(\delta) = \frac{I_1(0) + I_2(0)}{I_1(0) + I_2(0) \exp(\Gamma\delta)} \exp(-a\delta) \quad (2)$$

where Γ is the exponential gain coefficient for the signal beam in the coupling process, α is the exponential attenuation coefficient for the beam in the medium, δ is the thickness of the medium, $I_1(0)$ and $I_2(0)$ are the intensity of the incident signal beam and pump beam at the front surface of the medium, and $I_1(\delta)$ and $I_2(\delta)$ are the intensity of the two emergent beams at the back surface of the medium. It is worth noting that only when $\Gamma > \alpha$ can the signal beam have a positive gain. The formulas above represent the energy exchange that results from the two-light coupling.

Disregarding the Fresnel reflection losses and pump depletion, the pump beam intensities with and without coupling are approximate ($I_2(\delta) \approx I_2'(\delta)$), and the exponential gain coefficient Γ can be expressed as Formula (3) [20,21]:

$$\Gamma = \frac{1}{\delta} \ln \frac{I_1(\delta) I_2'(\delta)}{I_1'(0) I_2(\delta)} \approx \frac{1}{\delta} \ln \frac{I_1(\delta)}{I_1'(0)} \quad (3)$$

where $I_1'(0)$ and $I_2'(\delta)$ are the transmitted intensity of the signal and pump beam without coupling.

Using the Kr^+ laser as a light source, with $\lambda = 476$ nm, the polarization direction exists in the plane of incidence (e). The crossing angle between the incidence signal beam $I_1(0)$ and pump beam $I_2(0)$ is 2θ , the crystal medium thickness is $\delta = 1.0$ mm and the diameters of the signal light and pump light are $D = 0.8$ mm and $D = 3$ mm, respectively. The light passes through the γ face of the LiNbO_3 crystal. $I_2(0) = 1.52$ w/cm² and $I_2(0)/I_1(0) = 1240$. The experimental setup of two-wave coupling is shown in Figure 2.

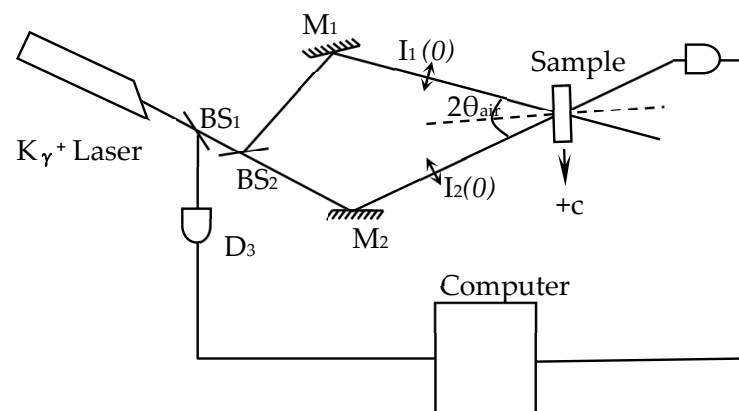


Figure 2. Experimental setup of two-wave coupling. M_1, M_2 : mirrors; BS_1, BS_2 : beam splitters; D_1, D_2 : photo detectors; $I_1(0)$: incident signal beam; $I_2(0)$: incident pump beam; $I_1(\delta)$: emergent signal beam after coupling.

The measurement results of the exponential gain coefficient Γ and response time τ_w of the RF1, RF2, RF3 and RF4 samples are listed in Tables 2 and 3.

Table 2. Experimental results of two-wave coupling of exponential gain coefficient of Sc:Ru:Fe:LiNbO_3 crystal.

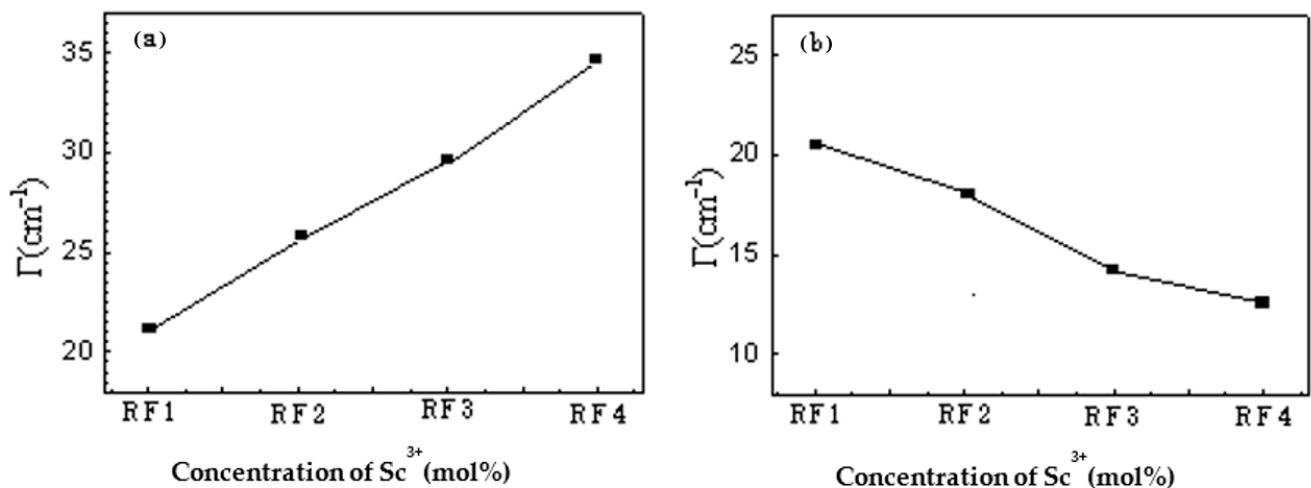
Samples	τ_w (s)	λ (nm)	δ (mm)	2θ (deg)	Γ (cm ⁻¹)
RF1	104	476	1.0	24.4	22.5
RF2	73	476	1.0	25.6	26.8
RF3	42	476	1.0	28.8	29.6
RF4	16	476	1.0	31.8	34.8

Table 3. Experimental results of two-wave coupling of exponential gain coefficient of Sc:Ru:Fe:LiNbO₃ crystal.

Samples	τ_w (s)	λ (nm)	δ (mm)	2θ (deg)	Γ (cm ⁻¹)
RF1	125	633	1.0	22.3	20.5
RF2	94	633	1.0	18.2	18.2
RF3	72	633	1.0	16.1	14.3
RF4	36	633	1.0	14.3	12.4

From Tables 2 and 3, we can conclude that using the Kr⁺ laser (476 nm blue light), the exponential gain coefficient Γ in Sc:Ru:Fe:LiNbO₃ with Sc³⁺ ion concentration increased from 24.4 cm⁻¹ for RF1 to 31.8 cm⁻¹ for RF4. Using the He-Ne laser (633 nm red light), the exponential gain coefficient Γ in Sc:Ru:Fe:LiNbO₃ with Sc³⁺ ion concentration decreased from 22.3 cm⁻¹ for RF1 to 14.3 cm⁻¹ for RF4.

In Figure 3, comparing the Γ at 476 nm of RF1 with the Γ at 633 nm of RF1, it increased by a factor of 1.09; the Γ at 476 nm of RF2 compared with the Γ at 633 nm of RF2 showed an increase by a factor of 1.40; the Γ at 476 nm of RF3 compared with the Γ at 633 nm of RF3 showed an increase by a factor of 1.78; and the Γ at 476 nm of RF4 compared with the Γ at 633 nm of RF4 showed an increase by a factor of 2.2.

**Figure 3.** Change in exponential gain coefficient Γ : (a) Kr⁺ laser (476 nm blue light) and (b) He-Ne laser (633 nm red light).

4. Blue Photorefractive Properties of the Sc:Ru:Fe:LiNbO₃ Crystal

The photorefractive properties of the Sc:Ru:Fe:LiNbO₃ crystal using the Kr⁺ laser ($\lambda = 476$ nm blue light) as a light source were investigated. The intensity of each beam of the Kr⁺ laser was about 140 mW/cm². The incidence angle was $\theta = 14^\circ$. The photorefractive properties were investigated using the two-beam coupling setup (see Figure 2). During recording, one of the writing beams was blocked intermittently, while the other writing beam served as a readout beam to measure the diffraction efficiency of the written grating. The diffraction efficiency η_s of the grating is defined as $\frac{I'_s}{I_s} \times 100\%$, where I'_s and I_s are the diffracted and transmitted light intensity, respectively. The temporal behavior of η_s during recording and erasing could be well described by the following functions [22]:

$$\sqrt{\eta(t)} = \sqrt{\eta_{sat}} [1 - \exp(-t/\tau_w)] \quad (4)$$

$$\eta(t) = \eta_{sat} \exp(-t/\tau_e) \quad (5)$$

where η_{sat} is the saturation diffraction efficiency during recording, and τ_w and τ_e are the recording (response time) and erasing time constants, respectively. Holographic data

storage systems have long held promise for their high storage capacity, short access times and high data transfer rates. For holographic storage systems, two of the most important system parameters are dynamic range, $M/\#$, and sensitivity, S . The larger the $M/\#$, the higher the storage density and the better the signal-to-noise ratio. Sensitivity determines the recording speed. The higher the sensitivity, the shorter the recording time required. $M/\#$ and S can be measured by single-hologram recording and erasure experiments. From the single hologram recording and erasure curve, we can calculate the $M/\#$ and S values using the following formulas:

$$M/\# = \frac{d\sqrt{\eta}}{dt}\bigg|_{t=0} \tau_e \approx \frac{\tau_e \sqrt{\eta_s}}{\tau_w} \quad (6)$$

$$S = \frac{d\sqrt{\eta/dt}\big|_{t=0}}{il} \approx \frac{\sqrt{\eta_s}}{\tau_w IL} \quad (7)$$

where τ_e is the erasure time constant and I and L are the total recording intensity and the thickness of the crystal, respectively. η_s is the maximal diffraction efficiency that is defined as the ratio of the diffraction light intensity to the transmission signal light intensity without a grating. The maximum refractive index change, Δn_{max} , can be calculated using the following equation:

$$\Delta n_{max} = \frac{\arcsin(\sqrt{\eta_s} \lambda \cos \theta)}{180 \times d} \quad (8)$$

where d is the thickness of the crystal, θ is the incident angle inside the crystal and λ is the wavelength outside the crystal. The maximum refractive index change Δn_{max} can be calculated from the measured maximum diffraction efficiency.

From the results in Tables 4 and 5, we can see that the Sc:Ru:Fe:LiNbO₃ crystals and Ru:Fe:LiNbO₃ crystals both represent strong blue photorefraction. Moreover, increasing the Sc³⁺ concentration could enhance the blue photorefraction significantly. For the photorefractive properties of RF4 in the Sc:Ru:Fe:LiNbO₃ crystal, the diffraction efficiency η_s reaches 75.7%, the response time τ_w shortens to 11 (s), the dynamic range $M/\#$ reaches 19.52, the photorefractive sensitivity reaches 2.85 (cm J⁻¹) and the maximum refractive index change Δn_{max} reaches 6.66×10^{-5} . With an increase in Sc³⁺ ion concentration, the diffraction efficiency (η_s), response time (τ_w), dynamic range ($M/\#$), sensitivity (s) and maximum refractive index change (Δn_{max}), from RF1 to RF4 under blue light irradiation, continually increase. Comparing Sc (3.0 mol%):Ru (0.1 wt%):Fe (0.06 wt%):LiNbO₃ (RF4) blue light with Ru: (0.1 wt%):Fe (0.06 wt%):LiNbO₃ (RF1), η_s is increased by a factor of 1.2, V_w (response rate) has a large increase by a factor of 22, $M/\#$ increases significantly by a factor of 6.8, S has a sharp increase by a factor of 23 and Δn_{max} increases by a factor of 1.1. Comparing the Kr⁺ laser (476 nm blue light) as a light source to record the holographic storage parameter of Sc (1 mol%):Ru (0.1 wt%):Fe (0.06 wt%):LiNbO₃ with a He-Ne laser (633 nm red light) as a source to record holographic storage parameters of Sc (1 mol%):Fe (0.06 wt%):LiNbO₃, η_s is increased by a factor of 1.9, V_w (response rate) is increased by a factor of 13.9, $M/\#$ increased significantly by a factor of 1.8, S sharply increased by a factor of 32 [23] and Δn_{max} improved by a factor of 1.4.

Table 4. The blue ($\lambda = 476$ nm) photorefractive properties of Sc:Ru:Fe:LiNbO₃ crystal.

Samples	η_s (%)	τ_w (S)	τ_e (S)	$M/\#$	S (cmJ ⁻¹)	Δn_{max} (10 ⁻⁵)
RF1	62.8	242	870	2.85	0.12	5.94
RF2	66.7	104	610	4.79	0.28	6.02
RF3	70.4	46	430	7.84	0.65	6.16
RF4	75.7	11	244	19.52	2.85	6.66

Table 5. The red (633 nm) photorefractive properties of Sc:Fe:LiNbO₃ crystal.

Samples	$\eta_S(\%)$	$\tau_w(S)$	$M/\#$	$S(\text{cmJ}^{-1})$	$\Delta n_{max} \times 10^{-5}$
Sc(1 mol%): Fe(0.06 wt%):LiNbO ₃	34.7	1450	2.66	0.0087	4.28

Blue Photorefractive Mechanisms in the Sc:Ru:Fe:LiNbO₃ Crystals

In the Sc:Ru:Fe:LiNbO₃ crystal, Ru and Fe for photorefraction play the dominant role. Sc³⁺ contributes to the photoconductivity, σ_{ph} . It is known that writing time is inversely proportional to the photoconductivity σ_{ph} according to the following equation [20]:

$$\tau_w \approx \frac{\epsilon\epsilon_0}{4\pi\sigma_{ph}} \quad (9)$$

Doping Sc³⁺ ions into the LiNbO₃ crystal induces an increase in photoconductivity σ_{ph} at the 476 nm wavelength, leading to a fast photorefractive response. It is worth emphasizing that blue light is short enough to excite charge carriers in both shallow and deep centers; thus, a grating can be directly recorded in the two centers with the same phase. Ascribed to the two centers' effect and in-phase merit at the 476 nm wavelength, the total intensity of the recorded grating is the sum of the two gratings recorded in the deep and shallow trap centers. Therefore, the photorefractive characteristics are improved dramatically compared with those in the single-center-doped LiNbO₃ crystals at the 476 nm wavelength. The mechanism of the blue photorefractive enhancement can be described as follows: doping Sc³⁺ ions into the Ru:Fe:LiNbO₃ crystal changes the occupied sites of the ions in the crystals. As a result, the concentrations of Ru_{Li}²⁺, Fe_{Li}^{+ / 2+} and Sc_{Li}²⁺ are changed. Moreover, a large coupling gain coefficient is observed, and the energy transferring direction is always in the +c-axis direction in blue photorefraction, indicating diffusion is the dominant charge transport mechanism and the light-excited holes are the dominant charge carriers. Such phenomena are different from those in red and green photorefraction. The factors mentioned above contribute to the significant enhancement of blue photorefractive properties when comparing the Ru:Fe:LiNbO₃ with the Sc:Ru:Fe:LiNbO₃ crystals.

5. Conclusions

Doped with 0.1 wt% RuO₂, 0.03 wt% Fe₂O₃ and 0, 0.5, 1.0 and 1.5 mol% Sc₂O₃, Sc:Ru:Fe:LiNbO₃ crystals were grown by using the Czochralski method. The types of dominant charge carriers were determined, and the holes were the dominant charge carriers under blue light irradiation, which is short enough to excite the charge carriers' holes in both shallow and deep trap centers. Therefore, the grating can be directly recorded in the two centers with the same phase. The maximum exponential gain coefficient Γ of RF4 under 476 nm irradiation reached 31.8 cm⁻¹. The Γ at 476 nm (blue light) of RF4 compared with the Γ at 633 nm (red light) of RF4 increased by a factor of 2.8. The exponential gain coefficient Γ at 476 nm (RF1, RF2, RF3 and RF4) continually increased. The photorefractive properties of η_S , τ_w , $M/\#$, S and Δn_{max} reached 75.7%, 11 s, 19.52, 2.85 cmJ⁻¹ and 6.66×10^{-5} . Comparing the Kr⁺ laser as a light source to record the holographic storage parameters of Sc(1 mol%):Ru(0.1 wt%):Fe(0.06 wt%):LiNbO₃ with the He-Ne laser as a source to record the holographic storage parameters of Sc(1 mol%):Fe(0.06 wt%):LiNbO₃, η_S increased by a factor of 1.9, V_w (response rate) increased by a factor of 13.9, $M/\#$ increased by a factor of 1.8, S increased by a factor of 32 and Δn_{max} improved by a factor of 1.4. This short wavelength recording in the two-center LiNbO₃ also offers a possible improvement for high-density volume holographic storage.

Author Contributions: Writing—original draft preparation, L.X.; Writing—review & editing, G.C. All authors have read and agreed to the published version of the manuscript.

Funding: This research was supported by 2019 Major Scientific and Technological Achievements Transformation Projects of Heilongjiang Province of China (Grant Number: CG20A008); 2021 Harbin Science and technology special plan project. Development of 8-inch silicon carbide (SiC) substrate material and equipment and Research on industrialization process (Grant Number: 2021ZSZZGH10) and Outstanding Young Scholars Project supported by the Natural Science Foundation of Heilongjiang Province, China. Research and development of PVT 2–4 inch AlN single crystal equipment and key technology (Grant Number: JQ2019E003).

Conflicts of Interest: The authors declare no conflict of interest.

References

1. Zhang, X.; Liang, G.J.; Xu, Z.P. Defect structure and holographic storage properties of $\text{LiNbO}_3\text{:Zr:Fe:Cu}$ crystals with various Li/Nb ratios. *Opt. Mater.* **2019**, *96*, 109318. [\[CrossRef\]](#)
2. Burr, G.W.; Jefferson, C.M.; Coufal, H.; Jurich, M.; Hoffnagle, J.A.; Macfarlane, R.M.; Shelby, R.M. Volume holographic data storage at an areal density of 250 gigapixels/in (2). *Opt. Lett.* **2001**, *26*, 444. [\[CrossRef\]](#)
3. Markov, V.; Millerd, J.; Trolinger, J.; Norrie, M.; Downie, J.; Timucin, D. Multilayer volume holographic optical memory. *Opt. Lett.* **1999**, *24*, 265–267. [\[CrossRef\]](#)
4. Buse, K.; Jermann, F.; Krätzig, E. Infrared holographic recording in $\text{LiNbO}_3\text{:Fe}$ and $\text{LiNbO}_3\text{:Cu}$. *Opt. Mater.* **1995**, *4*, 237–240. [\[CrossRef\]](#)
5. McMillen, D.K.; Hudson, T.D.; Wagner, J.; Singleton, J. Holographic recording in specially doped lithium niobate crystals. *Opt. Express* **1998**, *2*, 491–502. [\[CrossRef\]](#)
6. Sugak, D.; Buryy, O.; Sugak, Y.; Zhydachevskii, Y.; Beckere, K.-D.; Martynyuka, N.V.; Yakhnevycha, U.; Ubizskii, S. Optical in-situ study of the redox processes in $\text{LiNbO}_3\text{:Fe}$ crystals. *Opt. Mater.* **2019**, *99*, 109543. [\[CrossRef\]](#)
7. Fujimura, R.; Kubota, E.; Matoba, O.; Shimuraa, T.; Kuroda, K. Photorefractive and photochromic properties of Ru doped $\text{Sr}_{0.61}\text{Ba}_{0.39}\text{Nb}_2\text{O}_6$ crystal. *Opt. Commun.* **2002**, *213*, 373–378. [\[CrossRef\]](#)
8. Chiang, H.; Chen, J. Growth and properties of Ru-doped lithium niobate crystal. *J. Cryst. Growth* **2006**, *294*, 323–329. [\[CrossRef\]](#)
9. Wang, L.P.; Dai, L.; Liu, C.R.; Han, X.; Shao, Y.; Xu, Y. Investigation on the holographic storage properties varied with ZrO_2 co-doping in Ru: Fe: LiNbO_3 crystals. *Opt. Mater.* **2019**, *89*, 118. [\[CrossRef\]](#)
10. Dai, L.; Shao, Y.; Liu, C.R.; Chen, R.; Han, X.; Yang, S. Effect of Hf^{4+} concentration on defect structure and optical properties of Yb:Tm: LiNbO_3 crystals. *Opt. Mater.* **2019**, *95*, 109193. [\[CrossRef\]](#)
11. Yang, C.L.; Tu, X.N.; Wang, S.; Xiong, K.; Chen, Y.; Zheng, Y.; Shi, E. Growth and properties of Pr^{3+} doped LiNbO_3 crystal with Mg^{2+} incorporation: A potential material for quasi-parametric chirped pulse amplification. *Opt. Mater.* **2020**, *105*, 109893. [\[CrossRef\]](#)
12. Nakamura, M.; Takekawa, S.; Liu, Y.; Kitamura, K. Crystal growth of Sc-doped near-stoichiometric LiNbO_3 and its characteristics. *Cryst. Growth* **2005**, *281*, 549–555. [\[CrossRef\]](#)
13. Li, S.; Liu, S.; Kong, Y.; Xu, J.; Zhang, G. Enhanced photorefractive properties of $\text{LiNbO}_3\text{:Fe}$ crystals by HfO_2 codoping. *Appl. Phys. Lett.* **2006**, *889*, 101126. [\[CrossRef\]](#)
14. Zheng, W.; Liu, B.; Bi, J.C.; Xu, Y.H. Holographic associative memory by phase conjugate of four-wave-mixing in Sc:Fe: LiNbO_3 crystal. *Opt. Commun.* **2005**. [\[CrossRef\]](#)
15. Yang, M.M.; Long, S.W.; Zhu, Y.Z.; Ma, H.; Lin, S.; Quan, J.; Wang, B. Spectroscopic properties and thermally stable orange-red luminescence of Sm: Zr: LiNbO_3 and Sm: Hf: LiNbO_3 for white LED applications. *Ceram. Int.* **2020**, *47*, 1970–1975. [\[CrossRef\]](#)
16. Dai, L.; Wang, Y.N.; Chen, R.R.; Yang, S.; Han, X.; Liu, C.; Shao, Y. Dopant Occupancy and UV–Vis–NIR Spectroscopy of Sc: Yb: Tm: LiNbO_3 in the 300–3000 nm Wavelength Range. *Cryst. Res. Technol.* **2020**, *55*, 1900176. [\[CrossRef\]](#)
17. Qiao, H.; Xu, J.; Zhang, G.; Zhang, X.; Sun, Q.; Zhang, G. Ultraviolet photorefractivity features in doped lithium niobate crystals. *Phys. Rev. B* **2004**, *70*, 094101. [\[CrossRef\]](#)
18. Xu, C.; Xu, Z.P.; Fan, Y.X.; Xu, L.; Yang, C.H.; Xu, Y.H. Investigation on the blue photorefractive properties varied with MgO codoping in Ru:Fe: LiNbO_3 crystals. *Cryst. Res. Technol.* **2012**, *47*, 863–867. [\[CrossRef\]](#)
19. Dai, L.; Shao, Y.; Han, X.B.; Liu, C.; Wang, L. Effect of [Li]/[Nb] ratios on segregation coefficient and dopant occupancy of In: Yb: Nd: LiNbO_3 crystals. *Mod. Phys. Lett. B* **2019**, *13*, 1950160. [\[CrossRef\]](#)
20. Ewbank, M.D.; Neurgaonkar, R.R.; Cory, W.K.; Feinberg, J. Photorefractive properties of strontium barium niobite. *Appl. Phys.* **1987**, *62*, 373. [\[CrossRef\]](#)
21. Vazquez, R.A.; Neurgaonkar, R.R.; Ewbank, M.D. Photorefractive properties of SBN:60 systematically doped with rhodium. *Opt. Soc. Am. B* **1992**, *9*, 1416. [\[CrossRef\]](#)

22. Sun, X.D.; Luo, S.H.; Wang, J.; Jiang, Y.; Shi, H. Improvement of blue photorefractive properties in In-doped LiNbO₃:Fe:Cu crystals. *J. Phys. D Appl. Phys.* **2009**, *42*, 115413. [[CrossRef](#)]
23. Xua, Z.P.; Xua, S.W.; Zhang, J.; Liu, X.; Xu, Y. Growth and photorefractive properties of In:Fe:LiNbO₃ crystals with various [Li]/[Nb] ratios. *J. Cryst. Growth* **2005**, *280*, 227. [[CrossRef](#)]